

## Phase transition of CdS in the presence of ethylenediamine and formation of hollow CdS submicron particles with needle-like structure

Qingde Chen<sup>a</sup>, Huaying Bao<sup>a\*</sup> and Xinghai Shen<sup>b</sup>

<sup>a</sup>College of Chemistry, Beijing Normal University, Beijing 100875, P.R. China; <sup>b</sup>Beijing National Laboratory for Molecular Sciences, Department of Applied Chemistry, College of Chemistry and Molecular Engineering, Peking University, Beijing 100871, P.R. China

(Received 23 November 2007; final version received 13 March 2008)

Solid submicron particles, composed of amorphous, hexagonal and cubic phase CdS, were synthesized in water–ethylenediamine solution by precipitating Cd<sup>2+</sup> ions with S<sup>2-</sup> ions, which were generated from the radiolytic reduction of Na<sub>2</sub>S<sub>2</sub>O<sub>3</sub>. In addition, the effects of the absorbed dose on the crystallization process of CdS were investigated in detail. Moreover, hollow CdS submicron particles with needle-like structure could be obtained from the solid CdS submicron particles probably through a hollowing process based on Ostwald ripening and the phase transition of CdS from amorphous to crystalline. In the above processes, ethylenediamine played an important role.

**Keywords:** phase transition; crystal structure;  $\gamma$ -irradiation; cadmium sulfide

### 1. Introduction

As an important semiconductor with a wide band-gap energy (2.5 eV), CdS has attracted much attention because of their novel properties and possible application in both optoelectronic and biological fields [1–5]. It is well known that CdS has two common crystal structures, i.e., hexagonal phase and cubic phase, besides amorphous CdS. At relatively low temperature, cubic phase and amorphous CdS are easily obtained, while hexagonal phase CdS is not. As the properties of hexagonal phase CdS are much better than those of cubic phase CdS in the fields of photocatalysis [6,7], photoconduction [2,8] and so on, much efforts have been paid to the phase transition in CdS, i.e., amorphous to crystal [9,10] and cubic to hexagonal [4,11–18]. In the studies of the phase transition in CdS, the largest activity has been focused on the thermal treatment methods, such as thermal annealing [12–18] and hydrothermal treatment [9]. In addition, there are also reports about the laser or pressure induced phase transitions [19,20]. Generally, only the size of CdS nanoparticles increase after the phase transition [4,9,11,13,17,19].

In recent years, the self-assembly and highly-ordered organization of nanostructured building blocks into complex architectures have been of great interest in the areas of materials synthesis and nanodevice fabrication [21–28]. Especially, controlled organization into hollow and curved structures from rod-like building blocks is attractive to scientists not only because of its importance in understanding the concept of self-assembly with

---

\*Corresponding author. Email: hybao@bnu.edu.cn

artificial building blocks but also for its great application potential [24]. Cao et al. [24] synthesized hollow  $V_2O_5$  microspheres through the self-assembly of nanorods with poly(vinylpyrrolidone) micelles as templates in a ethylene glycol medium at  $140^\circ\text{C}$ , and the following calcination. In particular, Zhang et al. [27] obtained fluffy ZnS hollow microspheres (hexagonal phase) via the Ostwald ripening of the flower-like solid microspheres (hexagonal phase) at  $60^\circ\text{C}$ . However, to obtain the above flower-like solid ZnS microspheres, the concentrations of  $\text{Zn}^{2+}$ , ammonia and  $(\text{NH}_4)_2\text{SO}_4$  should be strictly controlled, and the synthesis process should take place at  $4^\circ\text{C}$  [27]. Otherwise, irregular aggregates of cubic phase ZnS were obtained [27]. If the above fluffy ZnS hollow microspheres could be synthesized from the easily synthesized cubic phase or amorphous ZnS at relatively low temperature, it will be interesting and practical. As to CdS, although a lot of references have reported how to control the morphologies of the nanoparticles and nanostructures [1–3], the reports on the template-free synthesis of the nanostructures with complex architectures at relatively low temperature are still scarce in the literature. Therefore, it is worthwhile exploring the synthesis of complex three-dimensional CdS nanostructures by using phase transition in solution at room temperature.

$\gamma$ -Irradiation has been widely used in preparing nanoparticles [29,30]. Recently, our research group has successfully synthesized Ag and Cu nanoparticles [31,32], octahedron  $\text{Cu}_2\text{O}$  nanocrystals [33], solid and hollow  $\text{Cu}_2\text{O}$  nanocubes [34] in water-in-oil microemulsions and Ag-poly(4-vinylpyridine) hybrid microgels [35,36] in surfactant-free aqueous solution. In addition, it has been proved that  $\gamma$ -irradiation can also be used to synthesize metal sulfide nanoparticles. For example, CdS nanoparticles (cubic phase) were synthesized in aqueous solution [37], while CdS nanoparticles (mixture of cubic and hexagonal phase CdS) were obtained in ethylenediamine (en) [38]. However, the generation course and the morphology transition were not studied in detail. In the present article, we report the syntheses and the generation course of the solid submicron particles, composed of amorphous, hexagonal and cubic phase CdS, in water-ethylenediamine solution by  $\gamma$ -irradiation. Then, the hollow CdS submicron particles with needle-like structure are further obtained through the Ostwald ripening and the phase transition of CdS from amorphous to crystalline with the assistance of ethylenediamine.

## 2. Materials and methods

### 2.1. Chemicals

Cadmium sulphate, sodium thiosulfate and ethylenediamine (en) of AR grade were used as received. Deionized and tri-distilled water was used in the experiments.

### 2.2. Synthesis of CdS submicron particles

An aqueous solution containing  $4\text{ mmol L}^{-1}$   $\text{CdSO}_4$ ,  $4.2\text{ mmol L}^{-1}$   $\text{Na}_2\text{S}_2\text{O}_3$  and  $1.6\text{ mol L}^{-1}$  ethylenediamine was prepared. After bubbling with high-purity  $\text{N}_2$  under anaerobic conditions for 20 min, the solution was irradiated in the field of a  $^{60}\text{Co}$   $\gamma$ -ray source for a definite time at a special location whose dose rate was determined by a ferrous sulfate dosimeter. The absorbed dose was 20 kGy and the dose rate was 20 Gy/min unless otherwise stated.

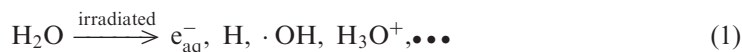
After irradiation, the obtained yellow precipitate was kept in a certain solution away from light at room temperature for a definite time. Except as stated otherwise, the ripening process took place in the mother solution and the aging time was 60 days. Then, the ripened sample was obtained.

### 2.3. Characterization

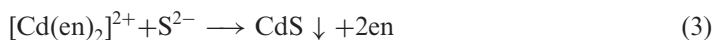
After irradiation or ripening, the precipitates were washed with water, and then dispersed in water. The obtained dispersion was dropped onto a Formvar-covered copper grid that was placed on a filter paper. After the solvent was evaporated at room temperature, the transmission electron microscopy (TEM) and selected area electron diffraction (SAED) images were conducted on a JEOL JEM-200CX microscope operated at 160 kV, the high-resolution TEM (HRTEM) images were performed on a Hitachi 9000 transmission electron microscope operated at 300 kV, and the scanning electron microscopy (SEM) images were obtained via a Hitachi S-4800 scanning electron microscope operated at 1.0 kV. The range of particle sizes was determined by measuring the dimensions of more than 100 particles based on the obtained micrographs. After the dispersed sample was deposited on a piece of glass, powder X-ray diffraction (XRD) pattern was recorded on an X'Pert PRO MPD diffractometer with Cu K $\alpha$  radiation ( $\lambda = 0.15418$  nm) and X-ray photoelectron spectrum (XPS) was collected on a Kratos Axis Ultra spectrometer with monochromatized Al K $\alpha$  radiation. After the dispersion was lyophilized, UV-Vis diffuse reflectance spectrum (DRS) of the solid sample was obtained by a UV-Vis-NIR spectrophotometer (JASCO V-570) equipped with an integrating sphere assembly.

### 3. Results and discussion

As well known, when an aqueous solution is irradiated by  $\gamma$ -rays, the water molecules absorb most of the irradiation energy and generate the reactive species, i.e., hydrated electron ( $e_{\text{aq}}^-$ ), H,  $\cdot\text{OH}$  and so on (Equation (1)) [39]:



Then, the reducing species, especially  $e_{\text{aq}}^-$ , reduce  $\text{S}_2\text{O}_3^{2-}$  ions to  $\text{S}^{2-}$  ions (Equation (2)) [40], which react with  $[\text{Cd}(\text{en})_2]^{2+}$  ions to generate CdS (Equation (3)).



Furthermore, besides coordinating with  $\text{Cd}^{2+}$  and neutralizing  $\text{H}_3\text{O}^+$ , ethylenediamine can also scavenge  $\cdot\text{OH}$  (Equation (4)),



with a rate constant of  $5.5 \times 10^9 \text{ L mol}^{-1} \text{ s}^{-1}$  [39], which can eliminate the influence of  $\cdot\text{OH}$  on the formation of  $\text{S}^{2-}$  and favor the generation of CdS.

#### 3.1. Synthesis of solid CdS submicron particles

Figure 1(a) shows the TEM image of the fresh product synthesized by  $\gamma$ -irradiation. It can be seen that the product is composed of quasi-spherical solid submicron particles, with diameter of 50–700 nm, and the surface of few particles appears needle-like structure, which is confirmed by the corresponding SEM image (Figure 1(d)). Furthermore, many small tuber-like structures appear on the surface of most particles, which further form coral-like structure *via* aggregation (Figure 1(d)). The related TEM image in higher

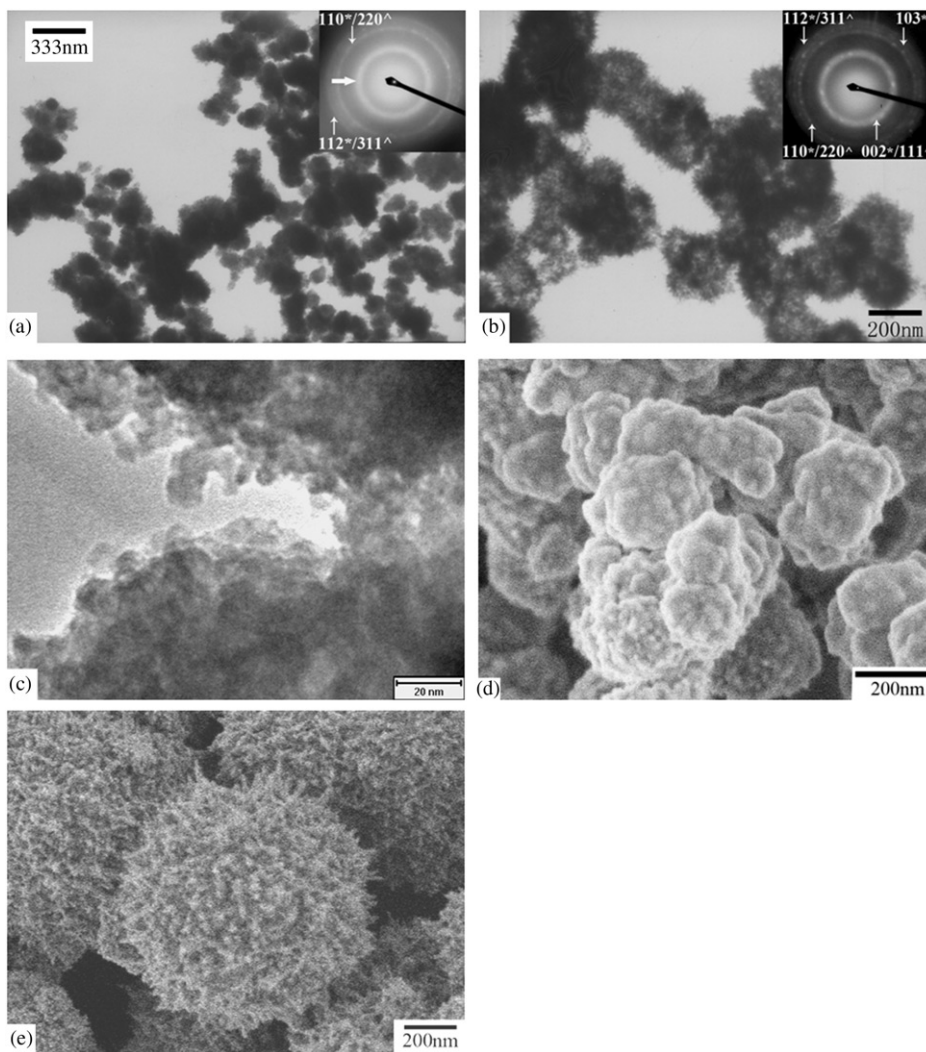


Figure 1. TEM (a–c) and SEM (d–e) images of the fresh (a, c, d) and ripened (b, e) samples.

Notes: The inset shows the SAED pattern of the corresponding product,

\*Represents hexagonal phase CdS,

^ Represents cubic phase CdS. (Absorbed dose: 20 kGy, dose rate: 20 Gy/min).

resolution (Figure 1(c)) further indicates that the surface of most submicron particles is quite coarse and they are comprised of numerous nanoparticles, with the diameter ranging from 5 to 10 nm. The corresponding XPS analysis (curves a in Figure 2) shows that the binding energies of S 2p<sub>3/2</sub>, S 2p<sub>1/2</sub>, Cd 3d<sub>5/2</sub> and Cd 3d<sub>3/2</sub> are 161.29, 162.46, 404.96 and 411.73 eV, respectively, close to the values reported in the literature [41], which indicates the generation of CdS.

In the corresponding XRD pattern (curve c in Figure 3), four broaden (102), (110), (103) and (112) diffraction peaks, corresponding to the hexagonal phase CdS structure, were observed. However, the existence of cubic phase CdS could not be excluded because the (110) and (112) diffraction peaks of hexagonal phase CdS overlap with the (220) and

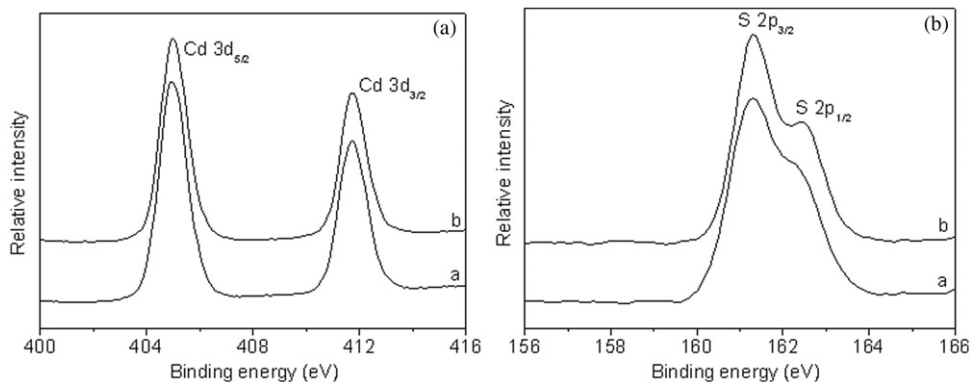


Figure 2. X-ray photoelectron spectra in the Cd 3d (a) and S 2p (b) regions for the fresh (line a) and ripened (line b) samples.

Note: Absorbed dose: 20 kGy, dose rate: 20 Gy/min.

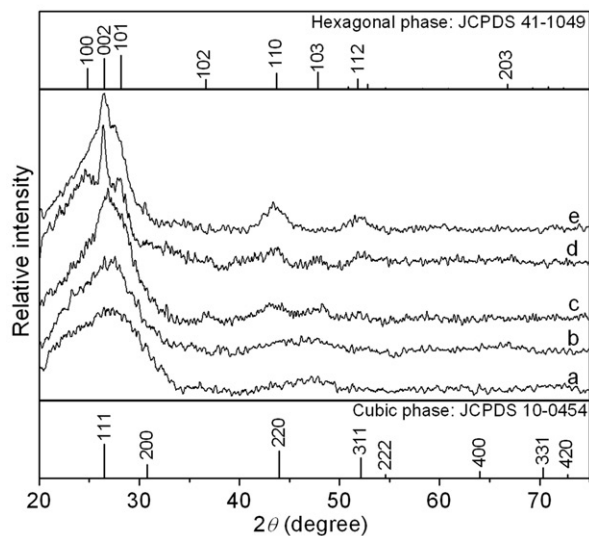


Figure 3. XRD patterns of the samples synthesized under different conditions: (a) 3 kGy, fresh; (b) 9 kGy, fresh; (c) 20 kGy, fresh; (d) 20 kGy, ripened; (e) 9 kGy, ripened.

Note: Dose rate: 20 Gy/min.

(311) diffraction peaks of cubic phase CdS, respectively. It is also noticed that the peak at  $\approx 27.3^\circ$  could not be ascribed to the (002) or (101) diffraction peak of hexagonal phase CdS, and not to the (111) diffraction peak of cubic phase CdS. This peak might have arisen from the scattering of amorphous CdS. The related SAED analysis (inset, Figure 1(a)) shows that there is an abroad noncrystalline ring (see the arrowhead in the inset of Figure 1(a)) besides two sharp diffraction rings, corresponding to (110) and (112) planes of hexagonal phase CdS or corresponding to (220) and (311) planes of cubic phase CdS. This indicates the coexistence of amorphous and crystal CdS. The HRTEM images of the as-prepared products shown in Figure 4(a) and (b) exhibit lattice fringes with *d* spacings of 0.29 and 0.25 nm, corresponding to (200) reflection of cubic phase CdS and (102) reflection

of hexagonal phase CdS, respectively, which indicates the coexistence of the two structures of CdS. Meanwhile, it can be found that the lattice fringes appear discontinuously, suggesting the presence of amorphous CdS.

According to the above discussion, it can be deduced that the fresh product is composed of amorphous, hexagonal and cubic phase CdS.

### 3.2. Formation of hollow CdS submicron particles with needle-like structure

The TEM image of the ripened sample (Figure 1(b)) shows a distinct contrast between the dark edge and the pale center in most particles, evidencing their hollow nature. At the same time, the surface of most particles appears obvious needle-like structure (Figure 1(b)), which has been further confirmed by the corresponding SEM image (Figure 1(e)). The corresponding XPS analysis (curves b in Figure 2) indicates that the product is still CdS. As shown in Figure 3 (curve d), besides those broaden hexagonal/cubic phase CdS diffraction peaks mentioned above, there are broaden (100), (002) and (101) diffraction peaks of hexagonal phase CdS, or (111) diffraction peak of cubic phase CdS in the XRD pattern of the as-prepared product. In the related SAED analysis (inset, Figure 1(b)), there is a sharp diffraction ring, corresponding to the (103) plane of hexagonal phase CdS, besides the diffraction rings mentioned above. Moreover, the noncrystalline ring becomes weak, in which there are many diffraction dots, corresponding to (002) plane of hexagonal phase CdS or (111) plane of cubic phase CdS. These indicate that more crystal CdS was generated during the period of ripening.

As shown in the typical HRTEM image (Figure 4(c)), clear lattice fringes with d spacing of 0.37 nm, corresponding to (100) reflection of hexagonal phase CdS, appear not

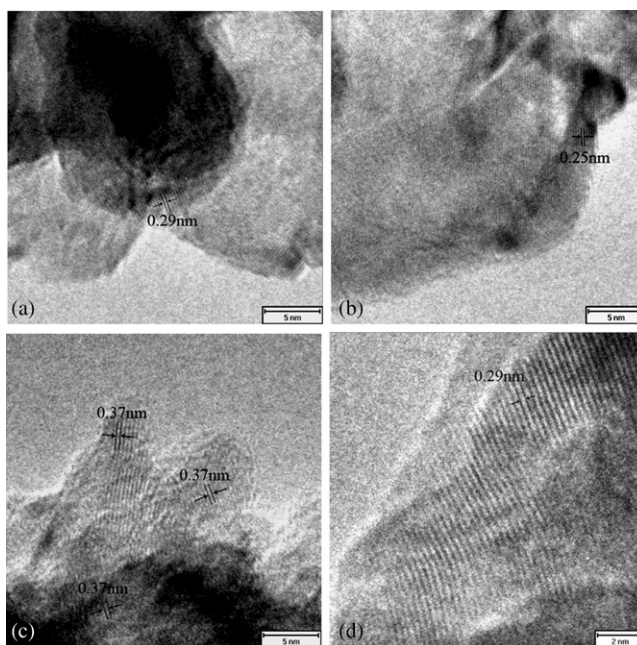


Figure 4. HRTEM images of the fresh (a, b) and the ripened (c, d) samples. Note: Absorbed dose: 20 kGy, dose rate: 20 Gy/min.

only in the needle-like structure but also in the basal body of the submicron particles. Moreover, cubic phase CdS only exists in a few bare particles (Figure 4(d)). It is worth noticing that the lattice fringes of the ripened sample appear more continuously than those of the fresh sample. Combining the disappearance of the peak at  $\approx 27.3^\circ$  in the corresponding XRD pattern (curve d in Figure 3) and the weakening of the non-crystalline ring in the related SAED pattern (inset, Figure 1(b)), it can be deduced that the crystal CdS, especially hexagonal phase CdS, is the main component of CdS submicron particles. In other words, the phase transition from amorphous to crystalline takes place in the period of ripening.

While the ripening temperature rose to  $60^\circ\text{C}$ , a similar morphology was obtained after 24 h (Supporting information, SI-1). Namely, the ripening process could be accelerated by raising the temperature.

### 3.3. Effects of the absorbed dose

Before further exploring the phase transition, the effects of the absorbed dose on the synthesis of CdS submicron particles were first studied in detail. At the absorbed dose of 3 kGy, obvious CdS exciton absorption, with an absorbed edge ( $\lambda_e$ ) of  $\approx 483$  nm, appears in the UV–Vis diffuse reflectance spectrum (curve a in Figure 5). When the absorbed dose increases to 9 and 20 kGy, the  $\lambda_e$  of the exciton absorption are red-shifted to  $\approx 494$  and 500 nm (curves c and d in Figure 5), respectively. According to the experimental correlation between  $\lambda_e$  and the average diameter for CdS nanoparticles [42], the average sizes of the CdS nanoparticles are estimated to be about 5.0, 5.7 and 6.2 nm when the absorbed doses are 3, 9 and 20 kGy, respectively. However, the particle sizes observed via TEM images (Figures 1(a), 6(a) and 6(b)) are much larger than those calculated via UV–Vis spectra, suggesting that the submicron particles are the aggregations of CdS nanoparticles. This is in good agreement with the result from the TEM image in higher resolution (Figure 1(c)).

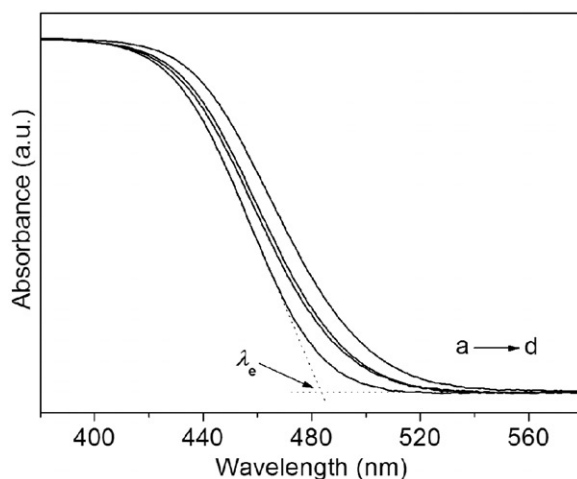


Figure 5. The effect of absorbed dose on the UV–Vis diffuse reflectance spectra of the solid samples: (a) 3 kGy, (b) 6 kGy, (c) 9 kGy, (d) 20 kGy.

Note: Dose rate: 20 Gy/min.

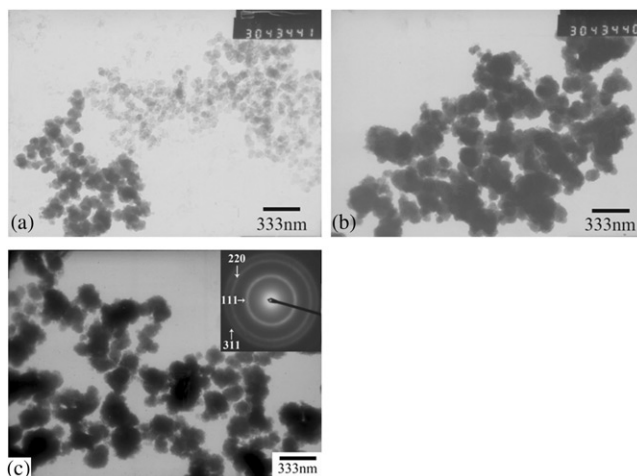


Figure 6. TEM images of the samples synthesized under different conditions: (a) 3 kGy, fresh; (b) 9 kGy, fresh; (c) 9 kGy, ripened.

Notes: The inset shows the SAED pattern of the corresponding product. (Dose rate: 20 Gy/min).

When the absorbed dose is 3 kGy, two broaden peaks at  $\approx 27.3^\circ$  and  $46.6^\circ$ , which are not related to the hexagonal phase or cubic phase CdS structure, appear in the corresponding XRD pattern (curve a in Figure 3). When the absorbed dose increases to 9 kGy, the two broaden peaks still exist, but become sharper (curve b in Figure 3). Especially, the peak at  $\approx 27.3^\circ$  does not disappear when the absorbed dose increases to 20 kGy (curve c in Figure 3). Furthermore, the related SAED analyses (not shown) indicate that the CdS obtained at the absorbed doses of 3 and 9 kGy are amorphous. Thus, it can be concluded that the CdS obtained at lower absorbed dose is amorphous and the two broaden peaks could arise from the scattering of amorphous CdS.

#### 3.4. Phase transition of amorphous CdS under different conditions

To study the phase transition, the amorphous CdS with an absorbed dose of 9 kGy was kept in mother solution for 24 h under the same ripening conditions as mentioned above. Then, a XRD pattern, similar to that of amorphous CdS, was obtained (not shown). This suggests that, under such conditions, the rate of phase transition is so slow that the amorphous CdS cannot be transformed to crystalline CdS in such a short time. Therefore, the crystal CdS in the fresh sample with the absorbed dose of 20 kGy is generated during the later stages of irradiation course because of the lower degree of supersaturation.

To further explore the effects of ethylenediamine on the phase transition, the identical amorphous CdS was washed sufficiently with water and then was kept in water for 60 days under the same ripening conditions. There appear not only the diffraction peaks, corresponding to the cubic phase CdS structure, but also the amorphous CdS scattering peak in the related XRD pattern (curve e in Figure 3). However, the (100), (101) or (103) diffraction peak, corresponding to the hexagonal phase CdS structure, is not observed. This indicates that only cubic phase CdS is generated via phase transition in the absence of ethylenediamine, which is further confirmed by the related SAED analysis (inset, Figure 6(c)). The corresponding TEM image (Figure 6(c)) shows that the CdS submicron particles are still solid and there is not needle-like structure on their surface.

### 3.5. Formation mechanism of hollow CdS submicron particles with needle-like structure

According to the above experimental results, it is suggested that the hollow CdS submicron particles with needle-like structure evolve from the solid submicron particles, composed of amorphous, hexagonal and cubic phase CdS, with the assistance of ethylenediamine.

Yang and Zeng [43] have obtained hollow TiO<sub>2</sub> nanospheres from solid nanospheres, aggregation of TiO<sub>2</sub> nanoparticles, via Ostwald ripening under hydrothermal conditions. They considered that the nanoparticles located in the inner cores have higher surface energies, compared with those in the outer surfaces [43]. Therefore, the inner nanoparticles are preferentially dissolved in the ripening course, resulting in the hollow interior [43]. Here, the solid submicron particles are comprised of numerous CdS nanoparticles. In the ripening course, a similar hollowing process may take place. Because ethylenediamine can coordinate with Cd<sup>2+</sup> and increase the dissolution rate and the solubility of CdS, the presence of ethylenediamine is propitious for this process. Then, CdS is precipitated again, in which ethylenediamine can favor the generation of hexagonal phase CdS [38]. Thus, the amorphous CdS could be transformed to crystal. Moreover, ethylenediamine could be preferentially absorbed on the growing surfaces parallel to a certain crystallographic direction of hexagonal phase CdS, resulting in the needle-like structure. While in the absence of ethylenediamine, the dissolving process of CdS becomes slower and water favors the generation of cubic phase CdS [38]. Therefore, the solid submicron particles, composed of cubic and amorphous phase CdS, are obtained. Combining the above discussion, it can be concluded that ethylenediamine plays an important role in the generation of hollow CdS submicron particles with needle-like structure.

## 4. Conclusions

Solid submicron particles, composed of amorphous, hexagonal and cubic phase CdS, were synthesized in water–ethylenediamine solution by precipitating Cd<sup>2+</sup> ions with S<sup>2-</sup> ions, which were generated from the radiolytic reduction of Na<sub>2</sub>S<sub>2</sub>O<sub>3</sub>. The crystalline CdS was generated during the later stages of irradiation course. Moreover, hollow CdS submicron particles with needle-like structure could be obtained from the solid CdS submicron particles probably through a hollowing process based on Ostwald ripening and the phase transition of CdS from amorphous to crystalline, where ethylenediamine played an important role. This process can be accelerated by rising the ripening temperature. According to our results reported herein, it is believed that complex three-dimensional architectures can be obtained by using Ostwald ripening and phase transition in the solution at room temperature, which will contribute in a new aspect to the construction of complex three-dimensional nanostructures.

## Acknowledgements

Sincere thanks are due to Ms Xiaoping Zhang (PKU) and Mr Gu Zhou (BNU) for help with TEM and SEM experiments, and to Mr Hui Ma (BNU) for help in XRD analysis. We also thank Dr Jinglin Xie (PKU) for help with XPS experiments and thank Mr Deliang Sun (PKU) for assistance in the  $\gamma$ -irradiation experiments.

## References

- [1] B.L. Cushing, V.L. Kolesnichenko, and C.J. O'Connor, *Recent advances in the liquid-phase syntheses of inorganic nanop articles*, Chem. Rev. 104 (2004), pp. 3893–3946.

- [2] T. Trindade, P. O'Brien, and N.L. Pickett, *Nanocrystalline semiconductors: Synthesis, properties, and perspectives*, Chem. Mater. 13 (2001), pp. 3843–3858.
- [3] C.D. Dushkin, S. Saita, K. Yoshie et al., *The kinetics of growth of semiconductor nanocrystals in a hot amphiphile matrix*, Adv. Colloid Interface Sci. 88 (2000), pp. 37–78.
- [4] R. Banerjee, R. Jayakrishnan, and P. Ayyub, *Effect of the size-induced structural transformation on the band gap in CdS nanoparticles*, J. Phys.: Condens. Matter 12 (2000), pp. 10647–10654.
- [5] A.P. Alivisatos, *Semiconductor clusters, nanocrystals, and quantum dots*, Science 271 (1996), pp. 933–937.
- [6] S. Yanagida, M. Kanemoto, T. Ogata et al., *Surface modified nano-space CdS microcrystallites. Third-order nonlinearity and photocatalysis*, in *New Funct. Mater*, C.T. Tsuruta, ed., Elsevier, Amsterdam, 1993, pp. 405–410.
- [7] M. Matsumura, S. Furukawa, Y. Saho et al., *Cadmium sulfide photocatalyzed hydrogen production from aqueous solutions of sulfite: effect of crystal structure and preparation method of the catalyst*, J. Phys. Chem. 89 (1985), pp. 1327–1329.
- [8] B. Dogil and M. Lepek, *Structural effect of cadmium sulfide thin films grown by a quasi-rheotaxy technique*, J. Mater. Sci. Lett. 12 (1993), pp. 1514–1515.
- [9] W.-W. So, J.-S. Jang, Y.-W. Rhee et al., *Preparation of nanosized crystalline CdS particles by the hydrothermal treatment*, J. Colloid Interface Sci. 237 (2001), pp. 136–141.
- [10] K. Kobayakawa, T. Miura, A. Suzuki et al., *Enhancement of the photocatalytic activity of cadmium sulfide powder for hydrogen evolution from aqueous sulfite solution by heat treatment with potassium chloride*, Sol. Energy Mater. Sol. Cells 30 (1993), pp. 201–209.
- [11] H. Tong and Y.-J. Zhu, *Synthesis of CdS nanocrystals based on low-temperature thermolysis of one single-source organometallic precursor*, Nanotechnology 17 (2006), pp. 845–851.
- [12] O. Zelaya-Angel and R. Lozada-Morales, *Sphalerite-wurtzite phase transformation in CdS*, Phys. Rev. B 62 (2000), pp. 13064–13069.
- [13] C. Ricolleau, L. Audinet, M. Gandais et al., *Structural transformations in II-VI semiconductor nanocrystals*, Eur. Phys. J. D 9 (1999), pp. 565–570.
- [14] K.L. Narayanan, K.P. Vijayakumar, K.G.M. Nair et al., *Structural transformation of dip coated CdS thin films during annealing*, J. Mater. Sci. 32 (1997), pp. 4837–4840.
- [15] R. Lozada-Morales and O. Zelaya-Angel, *Photoluminescence analysis of CdS thin films under phase transition*, Thin Solid Film 281–282 (1996), pp. 386–389.
- [16] O. Zelaya-Angel, L. Hernandez, O. de Melo et al., *Band-gap shift in CdS: phase transition from cubic to hexagonal on thermal annealing*, Vacuum 46 (1995), pp. 1083–1085.
- [17] R.J. Bandaranayake, G.W. Wen, J.Y. Lin et al., *Structural Phase-Behavior in II-VI Semiconductor Nanoparticles*, Appl. Phys. Lett. 67 (1995), pp. 831–833.
- [18] O. Zelaya-Angel, J.J. Alvarado-Gil, R. Lozada-Morales et al., *Band-gap shift in CdS semiconductor by photoacoustic spectroscopy: evidence of a cubic to hexagonal lattice transition*, Appl. Phys. Lett. 64 (1994), pp. 291–293.
- [19] M. Gajdardziska-Josifovska, V. Lazarov, J. Reynolds et al., *Wavelength dependence of laser-induced phase transformations in semiconductor quantum dots*, Appl. Phys. Lett. 78 (2001), pp. 3298–3300.
- [20] A.B. Herhold, C.C. Chen, C.S. Johnson et al., *Structural transformations and metastability in semiconductor nanocrystals*, Phase Transit. 68 (1999), pp. 1–25.
- [21] L.S. Zhong, J.S. Hu, H.P. Liang et al., *Self-assembled 3D flowerlike iron oxide nanostructures and their application in water treatment*, Adv. Mater. 18 (2006), pp. 2426–2431.
- [22] C. Diaz-Guerra, J. Piqueras, V. Popa et al., *Spatially resolved cathodoluminescence of GaN nanostructures fabricated by photoelectrochemical etching*, Appl. Phys. Lett. 86 (2005), Art. No. 223103.
- [23] N.G. Shang, C.P. Li, W.K. Wong et al., *Microstructure and field emission properties of coral-like carbon nanotubes*, Appl. Phys. Lett. 81 (2002), pp. 5024–5026.
- [24] A.M. Cao, J.S. Hu, H.P. Liang et al., *Self-assembled vanadium pentoxide ( $V_2O_5$ ) hollow microspheres from nanorods and their application in lithium-ion batteries*, Angew. Chem. Int. Edit. 44 (2005), pp. 4391–4395.

- [25] H.T. Shi, L.M. Qi, J.M. Ma et al., *Architectural control of hierarchical nanobelt superstructures in cationic reverse micelles*, *Adv. Funct. Mater.* 15 (2005), pp. 442–450.
- [26] T.X. Wang, A. Reinecke, and H. Colfen, *In situ investigation of complex BaSO<sub>4</sub> fiber generation in the presence of sodium polyacrylate. 2. Crystallization mechanisms*, *Langmuir* 22 (2006), pp. 8986–8994.
- [27] H.J. Zhang and L.M. Qi, *Low-temperature, template-free synthesis of wurtzite ZnS nanostructures with hierarchical architectures*, *Nanotechnology* 17 (2006), pp. 3984–3988.
- [28] G.M. Whitesides and B. Grzybowski, *Self-assembly at all scales*, *Science* 295 (2002), pp. 2418–2421.
- [29] A. Henglein, *Physicochemical properties of small metal particles in solution: “microelectrode” reactions, chemisorption, composite metal particles, and the atom-to-metal transition.*, *J. Phys. Chem.* 97 (1993), pp. 5457–5471.
- [30] J. Belloni, M. Mostafavi, H. Remita et al., *Radiation-induced synthesis of mono- and multi-metallic clusters and nanocolloids*, *New J. Chem.* 22 (1998), pp. 1239–1255.
- [31] P. He, X.H. Shen, and H.C. Gao, *Photoluminescence phenomenon during the formation of silver nanoparticles*, *Acta Phys. Chim. Sin.* 20 (2004), pp. 1200–1203.
- [32] Q.D. Chen, X.H. Shen, and H.C. Gao, *Formation of nanoparticles in water-in-oil microemulsions controlled by the yield of hydrated electron: The controlled reduction of Cu<sup>2+</sup>*, *J. Colloid Interface Sci.* 308 (2007), pp. 491–499.
- [33] P. He, X.H. Shen, and H.C. Gao, *Size-controlled preparation of Cu<sub>2</sub>O octahedron nanocrystals and studies on their optical absorption*, *J. Colloid Interface Sci.* 284 (2005), pp. 510–515.
- [34] Q.D. Chen, X.H. Shen, and H.C. Gao, *Formation of solid and hollow cuprous oxide nanocubes in water-in-oil microemulsions controlled by the yield of hydrated electrons*, *J. Colloid Interface Sci.* 312 (2007), pp. 272–278.
- [35] —, *One-step synthesis of silver-poly(4-vinylpyridine) hybrid microgels by  $\gamma$ -irradiation and surfactant-free emulsion polymerisation. The photoluminescence characteristics*, *Colloid Surf. A: Physicochem. Eng. Asp.* 275 (2006), pp. 45–49.
- [36] —, *One-step synthesis of silver-poly(4-vinylpyridine) hybrid microgels by  $\gamma$ -irradiation and surfactant-free emulsion polymerization*, *Acta Polym. Sin.* (2006), pp. 722–726.
- [37] Y. Yin, X. Xu, and Z. Zhang, *Synthesis of cadmium sulfide nanoparticles in situ using  $\gamma$ -radiation*, *Chem. Commun.* (1998), pp. 1641–1642.
- [38] M. Chen, Y. Xie, H.Y. Chen et al., *Preparation and characterization of metal sulfides in ethylenediamine under ambient conditions through a  $\gamma$ -irradiation route*, *J. Colloid Interface Sci.* 237 (2001), pp. 47–53.
- [39] G.V. Buxton, C.L. Greenstock, W.P. Helman et al., *Critical review of rate constants for reactions of hydrated electrons, hydrogen atoms and hydroxyl radicals in aqueous solution*, *J. Phys. Chem. Ref. Data* 17 (1988), pp. 513–886.
- [40] Y.H. Ni, X.W. Ge, H.R. Liu et al., *In situ synthesis and characterization of spherical CdS/polyacrylamide nanocomposites by gamma-irradiation in W/O microemulsions*, *Chem. Lett.* 30 (2001), pp. 924–925.
- [41] J.F. Moulder, W.F. Stickle, P.E. Sobol et al., *Handbook of X-ray Photoelectron Spectroscopy*, Perkin Elmer Physical Electronics Division, Eden, 1992.
- [42] M. Moffitt, H. Vali, and A. Eisenberg, *Spherical assemblies of semiconductor nanoparticles in water-soluble block copolymer aggregates*, *Chem. Mater.* 10 (1998), pp. 1021–1028.
- [43] H.G. Yang and H.C. Zeng, *Preparation of hollow anatase TiO<sub>2</sub> nanospheres via Ostwald ripening*, *J. Phys. Chem. B* 108 (2004), pp. 3492–3495.